

RESEARCH

Open Access



A coherent accumulation detection method based on SA-DPT for highly manoeuvring targets

Cunsuo Pang^{1,2*}, Huiling Hou¹ and Hualing Guo¹

*Correspondence:
pangcunsuo@126.com

¹ National Key Laboratory of Electronic Measurement Technology, North University of China, Taiyuan 030051, China
Full list of author information is available at the end of the article

Abstract

The emergence of highly manoeuvrable weak targets has led to serious degradation or even failure of traditional radar detection. In this paper, a coherent accumulation algorithm based on a combination of a scaling algorithm (SA) and a discrete polynomial-phase transform (DPT) is proposed, and the calculation burden and detection performance were evaluated. The algorithm first performs fewer speed parameter compensations based on an SA for the transmitted signal and selects the effective delay range of the target signal. Second, for the extracted echo signal, the DPT algorithm is used to estimate the target speed and acceleration. The proposed algorithm analyses the influence of the time delay range, the compensation speed and the delay unit on the detection performance and provides the improvement degree of the output SNR and the amount of complex multiplication. Finally, the experimental data verify the effectiveness of the proposed algorithm in terms of accumulation gain and parameter estimation. This method is for suboptimal estimation and requires much less computation than joint search methods, but it performs better than cross-correlation methods.

Keywords: Highly manoeuvring target, Weak signal detection, Scaling algorithm (SA), Discrete polynomial phase transform (DPT)

1 Introduction

With the development of aircraft technology, an increasing number of aircrafts have characteristics such as high speed, high manoeuvrability and stealth, which lead to great challenges to conventional radar detection. In addition, with the same observation time, the echo accumulation energy of a highly manoeuvrable target is about 20 dB lower than that of a conventional target in [1–3]. The echo of high manoeuvrable target is a nonlinear signal, and after FFT processing, it will appear the phenomenon of energy diffusion, which will also lead to the decline of detection probability.

Long-time accumulation, which includes coherent accumulation and noncoherent accumulation, is the common method to improve the target detection probability. Among them, the accumulation gain of the noncoherent accumulation method is low, and this paper mainly studies the coherent accumulation method. At present, there are

mainly two kinds of methods for long-time coherent accumulation [1–6]. One consists of the joint search methods based on parameters, which first estimate the range of target speed, acceleration and other parameters and then detect the target signal through a two-dimensional or multidimensional parameter search. For example, Li et al. [7] studied parameter compensation methods for speed and acceleration based on SA, improving the probability of target detection. Abatzoglou and Gheen [8] studied the parameter estimation methods for distance, speed, and acceleration based on the maximum likelihood estimator (MLE) and analysed the parameter errors using the Cramer–Rao Lower Bound (CRLB). Perry et al. [9], Sun et al. [10], Zheng et al. [11, 12] studied the compensation method for range migration (RM) based on the keystone (KT) method, but there were speed ambiguity numbers for the target with the higher speed. Sharif and Saman [13], Xu et al. [14], Yu et al. [15] and Xu et al. [16] studied highly manoeuvring target detection methods based on the Radon Fourier transform (RFT), which used the Radon transform and the FT to complete RM compensation and Doppler frequency migration compensation, respectively. Zheng et al. [17] studied the detection method for highly manoeuvring targets based on the three-dimensional scaled transform (TDST), which had an output signal-to-noise ratio (SNR) improved by more than 10 dB compared with that of the MTD method. Li et al. [18] studied the RM compensation based on the Radon transform and Doppler frequency migration compensation based on Lv's distribution (LVD), where the detection performance was close to that of the RFT. Tao et al. [19], Rao et al. [20], Chen et al. [21] and Pang et al. [22] studied the coherent accumulation method for high-speed targets based on the FRFT. Liu et al. [23] and Pang et al. [24] studied the sparse Fourier transform (SFT) method to accelerate the speed compensation and spectrum computation of high-speed targets.

Among the above methods, they had a high accumulation gain and good detection performance for low SNR signals, but they had a large calculation burden and poor real-time performance. To reduce the amount of computation, the other coherent accumulation method is the cross-correlation parameter estimation methods based on order reduction processing. This kind of method first performs cross-correlation processing on the target echo signal to realise the decoupling operation between speed and accumulation time, as well as dimension reduction processing. On this basis, it uses two-dimensional FFT to detect the target. For example, Wu et al. [25], Peleg and Friedlander [26], Liu et al. [27] and Pang et al. [28] studied highly manoeuvring target detection methods based on the discrete polynomial-phase transform (DPT). Niu et al. [29], Zheng [30], Li et al. [31, 32] and Zhang et al. [33] studied highly manoeuvring target detection methods based on the adjacent cross correlation function (ACCF). The second kind of method had the advantage of lower computational complexity than that of the first kind of method, but it required a higher input SNR than the first kind of method and was not suitable for detecting weak target signals.

Considering both the improvement of the detection performance and the reduction of the calculation burden, this paper focuses on analyzing the factors that degrade the detection performance of DPT in [26, 28]. To further improve the detection performance of the DPT method, a coherent accumulation detection method based on the combination of SA-DPT for highly manoeuvring targets is proposed in this paper, with its structure arranged as follows. The first part overviews the long-term coherent accumulation method commonly

used for weak signal detection, and analyses its detection performance and calculation burden. In the second part, the manoeuvring target echo model based on the LFM radar is given. In the third part, a long-time coherent accumulation method based on the combination of SA and DPT is proposed. In the fourth part, the implementation process of the proposed method is given, and the effects of the signal processing range, the speed compensation factor and the delay unit on the detection performance are analysed, while the complex multiplication operation of different methods are compared and analysed. In the fifth part, the experimental data is used to verify the effectiveness of the proposed method. The sixth part summarises and discusses the full text.

2 Highly manoeuvring target echo model

Assuming that the detection system is an LFM pulse radar, the frequency spectrum of the transmitted and received signals after down-conversion can then be expressed as follows [19]:

$$R(\hat{f}, n) = \frac{1}{\sqrt{\mu}} \text{rect}\left(\frac{\hat{f}}{\mu T_0}\right) \exp\left(-j\pi \frac{\hat{f}^2}{\mu}\right) \quad (1)$$

$$\begin{aligned} S(\hat{f}, n) = & \frac{A_0}{\sqrt{\mu}} \text{rect}\left(\frac{\hat{f} - f_d}{\mu T_0}\right) \exp\left[-j\pi \frac{(\hat{f} - f_d)^2}{\mu}\right] \\ & \times \exp(j2\pi f_d nT) \exp\left(-j\frac{4\pi R_0}{\lambda}\right) \\ & \times \exp[j\pi \alpha_d (nT)^2] \exp\left[-j2\pi (\hat{f} - f_d)(\tau_0 - \beta_0 nT)\right] \end{aligned} \quad (2)$$

where A_0 is the amplitude of the signal, μ is the frequency modulation rate, T_0 is the pulse width, R_0 is the initial range of the target distance from the radar, $\tau_0 = 2R_0/c$ is the initial time delay of the target, $\beta_0 = 2v_0/c$ is the time delay change rate of the target, $f_d = 2v_0/\lambda$ is the Doppler frequency of the target, $\alpha_d = 2a/\lambda$ is the first-order term of the Doppler frequency change, v_0 is the target radial speed, a is the target radial acceleration, T is the pulse repetition period, c is the velocity of light, f_c is the signal carrier, and $\lambda = c/f_c$ is the transmitted signal wavelength.

We multiply Eq. (1) by (2) to arrive at the frequency domain and time domain signals after pulse compression of the echo signal as follows:

$$\begin{aligned} X(\hat{f}, n) \approx & \frac{A_0}{\sqrt{\mu}} \text{rect}\left(\frac{\hat{f}}{B}\right) \exp[-j2\pi \hat{f}(\tau_0 - \beta_0 nT)] \exp\left(-j\frac{4\pi R_0}{\lambda}\right) \\ & \cdot \exp[j2\pi f_d(nT + \tau_0 - \beta_0 nT)] \exp[j\pi \alpha_d (nT)^2] \end{aligned} \quad (3)$$

$$x(\hat{t}, n) \approx A_0 \sqrt{D} \sin c \left[\pi B \left(\hat{t} - \tau_0 + \beta_0 n T + \frac{f_d}{\mu} \right) \right] \exp \left(-j \pi \frac{f_d^2}{\mu} \right) \cdot \exp \left(j \pi f_d \left(\hat{t} + \tau_0 - \beta_0 n T + \frac{f_d}{\mu} \right) \right) \exp (j 2 \pi f_d n T) \exp (j \pi \alpha_d (n T)^2) \quad (4)$$

where $D = B T_0$ is the product of the time width and the bandwidth; B is the bandwidth of the input signals.

It can be seen from Eqs. (3) and (4) that the exponential functions that cause the target envelope to produce time delay migration and Doppler frequency migration are as follows:

$$R(\hat{f}, \nu) = \exp[-j 2 \pi \hat{f} (\tau_0 - \Delta \tau)] \quad (5)$$

$$F(f_d, a) = \exp[j 2 \pi f_d (1 + \Delta f)] \quad (6)$$

where

$$\Delta \tau \approx \beta_0 n T \quad (7)$$

$$\Delta f \approx \alpha_d (n T) \quad (8)$$

Equations (7) and (8) show that in the same accumulation time, the greater the target speed and the acceleration are, the more serious the target energy diffusion, and therefore, the detection probability will fall substantially. The time delay migration caused by speed and the Doppler frequency migration caused by acceleration are mainly considered in this paper.

3 Coherent accumulation method based on the SA-DPT

To overcome the energy expansion caused by speed and acceleration, a coherent accumulation method based on the SA-DPT is proposed in this paper. The SA method can store the speed compensation factor and complete the speed compensation processing of the transmitted signal in advance, but the compensation processing mentioned in [2, 5–8] can complete the speed compensation after receiving the echo signal. Therefore, the SA method can improve the operation efficiency.

In addition, the delay range of the target after SA compensation is extracted; on this basis, the speed and acceleration information of the target can be obtained by using DPT. Compared with DPT processing in [27–29], the proposed method improves the detection probability of weak signals. At the same time, the operation of the proposed method is mainly a one-dimensional parameter search and two-dimensional FFT processing, and its amount of operation is much less than that in [5–8]. The proposed method provides a compromise in computational complexity, detection performance, and parameter estimation accuracy.

3.1 Speed compensation method based on the SA

(1) Speed compensation of transmitted signal

To correct the echo envelope range migration (RM) caused by $\sin c \left[\pi B \left(\hat{t} - \tau_0 + \beta_0 nT + \frac{f_d}{\mu} \right) \right]$ in Eq. (4) and improve the efficiency of the method, the SA method is used to compensate for the speed of the transmitted signal.

Equations (1)–(7) suggest that the factor that causes the target echo envelope to migrate is the exponential function term, $\exp(-j2\pi f \Delta \tau)$. Therefore, after speed compensation on Eq. (1), its expression can be written as follows:

$$R'(\hat{f}, n) = R(\hat{f}, n) * \omega(\hat{f}, n) \quad (9)$$

where

$$\begin{aligned} \omega(\hat{f}, n) &= \exp(j2\pi \hat{f} \Delta \tau) \\ &= \exp(-j2\pi \hat{f} \beta'_0 nT) \end{aligned} \quad (10)$$

In (10), $\beta'_0 = \frac{2\tilde{v}}{c}$, \tilde{v} is the speed compensation value.

Substituting (10) for (1), Eq. (4) can be rewritten as:

$$\begin{aligned} x(\hat{t}, n) &\approx A_0 \sqrt{D} \sin c \left[\pi B \left(\hat{t} - \tau_0 + \Delta \beta nT + \frac{f_d}{\mu} \right) \right] \exp \left(-j\pi \frac{f_d^2}{\mu} \right) \\ &\quad \cdot \exp \left(j\pi f_d \left(\hat{t} + \tau_0 - \Delta \beta nT + \frac{f_d}{\mu} \right) \right) \exp(j2\pi f_d nT) \exp(j\pi \alpha_d (nT)^2) \end{aligned} \quad (11)$$

where $\Delta \beta = \beta_0 - \beta'_0$.

After MTD for Eq. (11), it can be approximately expressed as:

$$\begin{aligned} z(\hat{t}, f) &\approx A_0 \sqrt{D} \left| \sum_{n=0}^{N-1} \sin c \left[\pi B \left(\hat{t} - \tau_0 + \Delta \beta nT + \frac{f_d}{\mu} \right) \right] \exp \left(-j\pi \frac{f_d^2}{\mu} \right) \right. \\ &\quad \cdot \exp \left(j\pi f_d \left(\hat{t} + \tau_0 - \Delta \beta nT + \frac{f_d}{\mu} \right) \right) \exp(j2\pi f_d nT) \exp(j\pi \alpha_d (nT)^2) \Big| \end{aligned} \quad (12)$$

In (12), the closer β_0 is to β'_0 , the smaller the RM of the echo envelope is, which is more conducive to the detection of the target. Next, the selection method of speed parameters \tilde{v} in Eq. (12) is given.

(2) Selection of \tilde{v}

If the envelope migration is less than a distance unit, the relationship among the speed compensation factor and the target speed and accumulation time NT in (12) can be expressed as follows:

$$\frac{\Delta v}{2} NT \leq \frac{c}{2f_s}, \quad \Delta v = \tilde{v} - v_0 \quad (13)$$

It can obtain from (13) as follows:

$$\Delta v \leq \frac{c}{NTf_s} \quad (14)$$

We let the target maximum speed be v_{\max} . The range of \tilde{v} is as follows:

$$\tilde{v} \in [0, \pm\Delta v, \dots, \pm Q\Delta v], \quad Q = \left\lfloor \frac{v_{\max}}{\Delta v} \right\rfloor \quad (15)$$

Equation (15) gives the compensation speed range and step interval. To quickly acquire the compensation range of the speed, the speed is searched using the binary search technique; then, the Q in (15) can be rewritten as follows:

$$Q = \left\lfloor \frac{v_{\max}/2^z}{\Delta v} \right\rfloor * \Delta v, \quad z = 1, 2, 3, \dots \quad (16)$$

3.2 Target detection and parameter estimation based on DPT

In (12), only speed compensation processing can be completed, but when the target acceleration becomes larger, the accumulated energy of the echo signal in (12) seriously diffuses. When the first kind of method in the introduction is used for processing, the amount of calculation is large, and the real-time performance is poor. Therefore, considering the advantages of the first kind of method and the second kind of method, this paper proposes to use (12) to first obtain the time delay estimation range of the target, then to carry out DPT to the signal within this range to complete the target detection. Then, the information, such as speed and acceleration is obtained.

3.2.1 Estimation of delay range

After finding the maximum value in (12), the target delay position can be estimated from the peak corresponding to the parameter. This process can be expressed as follows:

$$\Delta \hat{\tau} = \arg \max_l [z(\hat{t}, f_l)] \quad (17)$$

where $\Delta \hat{\tau}$ is the time delay estimation of the initial position of the target. The corresponding range is as follows:

$$\Delta \tau' \in [\Delta \hat{\tau} - b, \Delta \hat{\tau} + b] \quad (18)$$

where b can be set according to Eq. (7).

After selecting the target signal in (11) using Eq. (18), Eq. (11) can be modified as follows:

$$\begin{aligned} x(t', n) \approx & A_0 \sqrt{D} \sin c \left[\pi B \left(t' - \tau_0 + \Delta \beta n T + \frac{f_d}{\mu} \right) \right] \exp \left(-j\pi \frac{f_d^2}{\mu} \right) \\ & \cdot \exp \left(j\pi f_d \left(t' + \tau_0 - \beta_0 n T + \frac{f_d}{\mu} \right) \right) \exp(j2\pi f_d n T) \exp(j\pi \alpha_d (n T)^2). \end{aligned} \quad (19)$$

3.2.2 Target detection based on DPT

(1) Speed and acceleration estimation based on DPT

If the IFFT transformation is performed on (19), the frequency domain expression of the signal can be obtained as follows:

$$X(f', n) \approx \frac{A_0}{\sqrt{\mu}} \text{rect}\left(\frac{f'}{B}\right) \exp[-j2\pi f'(\tau_0 - \Delta\beta nT)] \exp\left(-j\frac{4\pi R_0}{\lambda}\right) \cdot \exp[j2\pi f_d(nT + \tau_0 - \Delta\beta nT)] \exp[j\pi\alpha_d(nT)^2] \quad (20)$$

Considering the influence of noise, after cross-correlation processing of (20) by column, the equation can be obtained as follows:

$$\begin{aligned} C(f', n, \tau_N) &= X(f', n) * X(f', n - \tau_N) \\ &= A_1 \text{rect}\left(\frac{f'}{B}\right) \exp[j2\pi f'(\Delta\beta\tau_N T - 2\tau_0)] \exp[j2\pi\alpha_d\tau_N T(nT)] \\ &\quad \cdots + w(f', n'), n' \in [1, N - \tau_N] \end{aligned} \quad (21)$$

where $A_1 = \frac{A_0^2}{\mu} \exp(-j\frac{8\pi R_0}{\lambda}) \exp(j4\pi f_d\tau_0) \exp[-j\pi\alpha_d(\tau_N T)^2]$, w is Gaussian noise with a 0 mean and a variance of σ^2 , and $\tau_N = \eta N$, $\eta \in (0, 1)$ is the delay unit relative to N .

When performing IFFT and FFT processing on f', n in (21), the equation can be obtained as follows:

$$\begin{aligned} z'(t', f_a, \tau_N) &= \text{FFT}_n[\text{IFFT}_{f'} C(f', n, \tau_N)] \\ &= A_1(N - \tau_N) \sin c[B(t' - \Delta\beta\tau_N T)] \\ &\quad \cdot \sin c[T_{\tau_N}(f_a - \alpha_d\tau_N T)] + w(t', n') \end{aligned} \quad (22)$$

where $T_{\tau_N} = (N - \tau_N)T$.

According to the results of (10) and (22), the values of the target velocity and acceleration can be approximately expressed as follows [28]:

$$\hat{v}' = \frac{c}{2\tau_N T} \frac{1}{f_s} \Delta m + \tilde{v} \quad (23)$$

$$\hat{a}' = \frac{\lambda}{2T^2} \frac{1}{(N - \tau_N)\tau_N} \Delta n \quad (24)$$

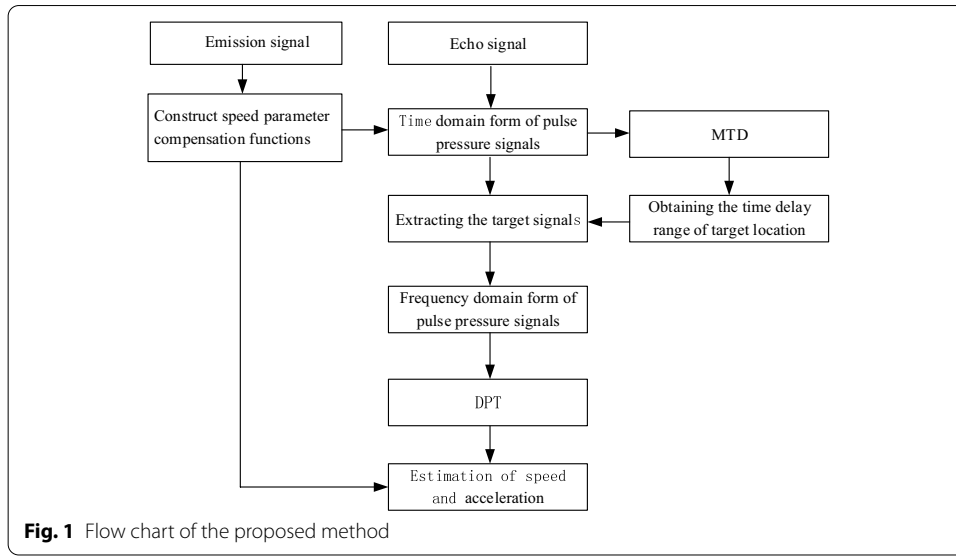
where Δm and Δn represent the time delay position and the Doppler frequency position, respectively, in (22), and \tilde{v} is the compensation value of the speed in (10).

According to \hat{v}' and \hat{a}' , the compensation function $\exp(-j2\pi f' \frac{2\hat{v}'}{c} nT) \exp[-j\pi \frac{2\hat{a}'}{c} (nT)^2]$ is constructed and is substituted into Eq. (3). Parameters, such as the distance and speed of the target can be obtained by using the MTD method.

The implementation process of the above method is shown in Fig. 1.

(2) Analysis of the output SNR

Due to cross correlation, the output noise power of DPT in [26, 28] is directly proportional to δ^2 . The larger δ^2 is, the higher the noise output power is, the lower the detection performance is, and vice versa. Therefore, this paper studies the change of δ^2 by changing the range of analysis signal.



In (22), the echo output power $P_{\text{out}|\text{signal}}$ and noise power $P_{\text{out}|\text{noise}}$ can be expressed as follows [26]:

$$P_{\text{out}|\text{signal}} = [\Delta\tau'(N - \tau_N)]^2 A_0^4 \quad (25)$$

$$\begin{aligned} P_{\text{out}|\text{noise}} &= \Delta\tau' \sum_{n=1}^{N-\tau_N} |A_0^2 \delta^2 + \delta^2 + \delta^4| \\ &= \Delta\tau'(N - \tau_N)(2A_0^2 \delta^2 + \delta^4) \end{aligned} \quad (26)$$

By combining Eqs. (25) and (26), the output SNR can be obtained as follows:

$$\begin{aligned} \text{SNR}_{\text{out}} &= \frac{P_{\text{out}|\text{signal}}}{P_{\text{out}|\text{noise}}} \\ &= \frac{N\Delta\tau'}{2} \frac{\text{SNR}_{\text{in}}^2}{1 + 2\text{SNR}_{\text{in}}} \Big|_{\tau_N=\frac{1}{2}}, \quad \text{SNR}_{\text{in}} = A_0^2/\delta^2 \end{aligned} \quad (27)$$

Comparing the output SNR in (27) with the output SNR of the DPT in [26, 28], the equation can be obtained as follows:

$$\Delta\text{SNR} \approx \frac{\Delta\tau' \text{SNR}_{\text{in}}^2 \Big|_{\tau_N=\frac{1}{2}}}{M \text{SNR}_{\text{in}}'^2 \Big|_{\tau_N=\frac{1}{2}}} \quad (28)$$

where $\text{SNR}' = A_0^2/\delta_0^2$, δ_0^2 is the noise variance of the DPT in [26], and the relationship with δ^2 in this paper is as follows:

$$\delta^2 = \frac{\Delta\tau'}{M} \delta_0^2 \quad (29)$$

Substituting (29) into (28), the equation can be obtained as follows:

$$\begin{aligned}\Delta \text{SNR} &\approx \frac{\Delta \tau'}{M} \left(\frac{\delta_0^2}{\delta^2} \right)^2 \\ &= \frac{M}{\Delta \tau'}\end{aligned}\quad (30)$$

According to Eq. (30), the smaller $\Delta \tau'$ is, the more obvious the improvement of the output SNR, which is more conducive to the detection of weak signals.

3.2.3 Performance analysis of the proposed method

(1) The influence of \hat{v} on the detection performance

We suppose that the carrier frequency of the radar is 3 GHz, the pulse repetition period is 3 ms, the number of accumulated pulses is 128, the signal bandwidth is 5 MHz, the baseband sampling rate is 10 MHz, the target is a point target, the maximum radial speed is 1000 m/s, the maximum radial acceleration is 10 m/s², and the SNR is −30 dB, $\Delta \tau' = 20$. Figure 2 shows a comparative analysis of the detection performance of the proposed method with different \hat{v} values. In addition, Fig. 2a shows that there is little

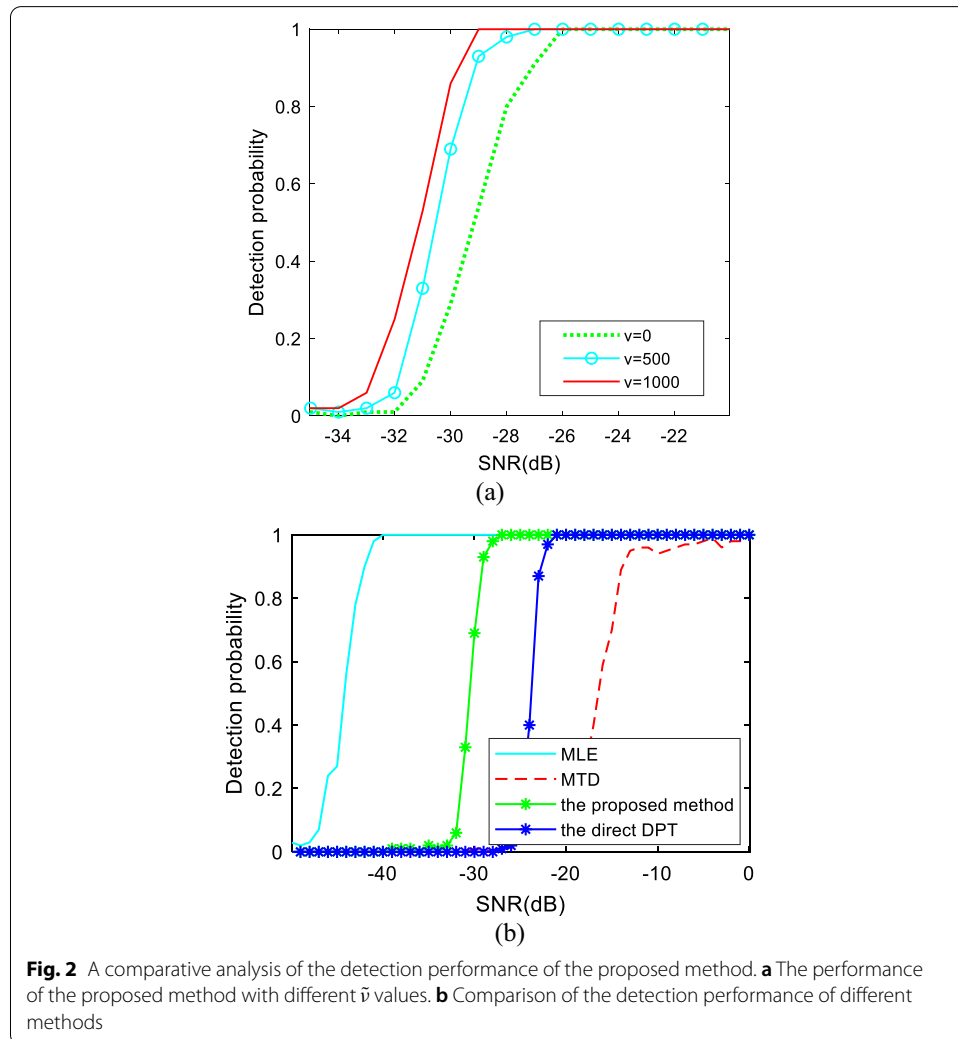


Fig. 2 A comparative analysis of the detection performance of the proposed method. **a** The performance of the proposed method with different \hat{v} values. **b** Comparison of the detection performance of different methods

difference in detection performance when the speed compensation value is 500 m/s and 1000 m/s, which shows that the proposed method has great adaptability to the speed compensation value; this can improve the execution efficiency of the method. Under the same conditions, the speed search times of the proposed method are approximately 30% less than those of MLE. Figure 2b shows that when the detection probability is 80%, with the proposed method, the input SNR is approximately 10 dB higher than with the MLE and approximately 5 dB lower than with the DPT, indicating that the detection performance of the proposed algorithm is between the two.

(2) Influence of $\Delta\tau'$ on the detection performance

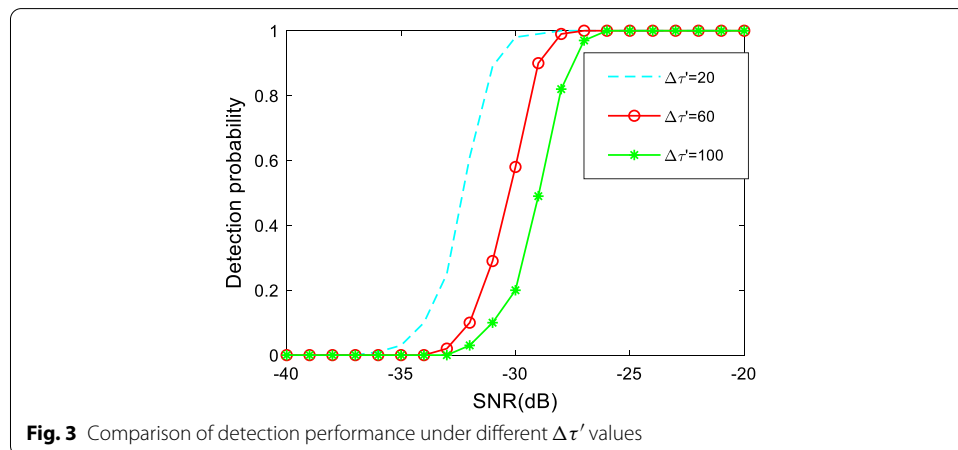
Figure 3 shows the comparison of the detection performance under different $\Delta\tau'$ values, from which it can be seen that the smaller $\Delta\tau'$ is, the better the detection performance. When the detection probability is 80%, the requirement for the input SNR when $\Delta\tau'$ is 20 is approximately 5 dB lower than that when $\Delta\tau'$ is 100, which is basically consistent with the theoretical value of Eq. (30), and it is more conducive to the detection of weak signals.

(3) The influence of τ_N on detection performance

Figure 4 shows the detection performance analysis of the proposed method with different τ_N values, from which it can be seen that the larger τ_N is, the greater the required input SNR with the same detection probability, but the relative estimation error of speed and acceleration is smaller. In contrast, the smaller τ_N is, the smaller the required input SNR is with the same detection probability, but the relative estimation error of speed and acceleration is larger. To facilitate the detection of weak signals, τ_N can be set as $(0.1 \sim 0.5)N$.

4 Complexity analysis of the proposed method

In what follows, the computational complexities of the MLE, KT, the direct DPT, and the proposed method are analysed. We assume that M and N denote the number of range cells and the number of pulses, k represents the number of speed compensations in the MLE and KT, and k' represents the number of speed compensations in the proposed method, where $k' \ll k$. With the proposed method, the phase compensation of the transmitted signal occurs before the pulse pressure, and therefore,



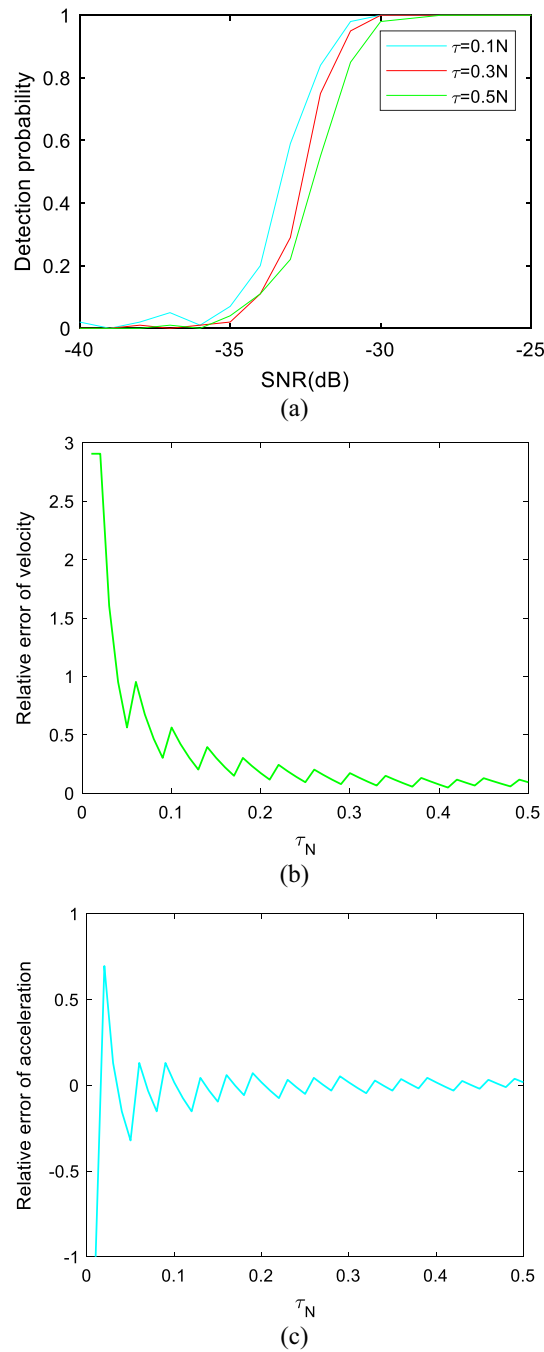
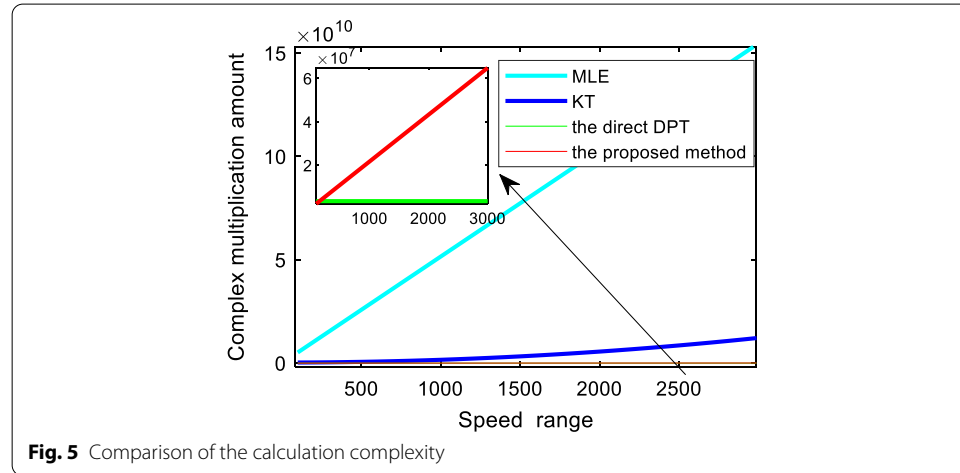


Fig. 4 The detection performance and parameter estimation of the proposed method with different τ_N values. **a** Detection performance with different τ_N values, **b** error of speed estimation, and **c** error of acceleration estimation

its calculated value can be stored in the register beforehand. The pulse pressure processing after one speed compensation requires $O(MN \log_2 M)$ complex multiplication operations, and one cross-correlation operation involves $O(MN \log_2 MN)$ complex multiplication operations. Thus, the amount of complex multiplication required for k'

Table 1 Complex multiplication amount of different methods

Methods	Computational complexity
MLE	$O(kNM^2 \log_2 N)$
KT	$O(NM^2) + O(k^2NM \log_2 M)$
the direct DPT	$O(NM \log_2 MN)$
Proposed method	$O(k'NM \log_2 MN)$


Fig. 5 Comparison of the calculation complexity

times of speed compensation is approximately $O(k'MN \log_2 MN)$. The detailed computational costs of the above mentioned methods are shown in Table 1 and Fig. 5. Table 1 shows that, in addition to the direct DPT, the proposed method has obvious advantages over other methods in terms of a complex multiplication burden. As seen from Fig. 5, as the speed increases, the computational advantage of the proposed method becomes more obvious. Therefore, combined with the results in Table 1 and Fig. 5, it can be seen that the proposed method has a good balance in detection performance and real-time performance; thus, this is conducive to the detection of weak target signals and the simultaneous real-time realisation.

5 Experimental results and discussion

To further verify the performance of the method, the simulation and measured data are analysed.

5.1 Implementation process of the proposed method

To clearly understand the execution process of the proposed method, the relevant processing results are given in Fig. 6. We let the simulation parameters be the same as those in 3.2.3, and we let $\Delta\tau' = 10$, $\tau_N = 0.5$. Figure 6a shows the MTD results, and Fig. 6b shows the direct DPT results in [26], from which it can be seen that the target signal is difficult to find. Figure 6c shows the MTD results based on SA, from which it can be seen that the SNR of the echo signal is higher than that of Fig. 6a, but the energy diffusion is

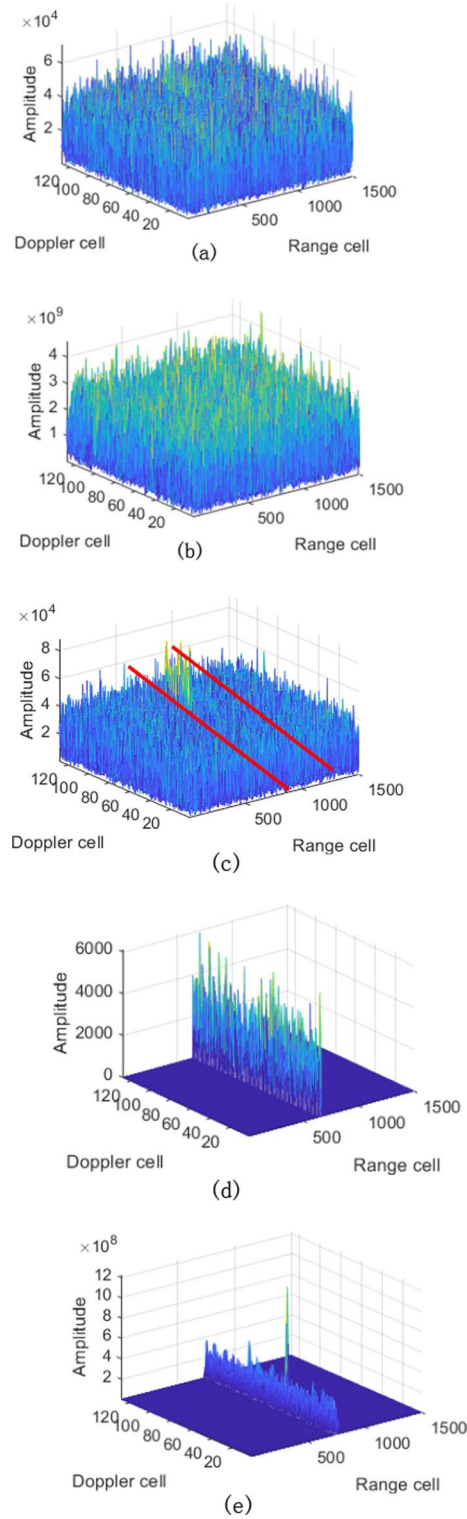


Fig. 6 The execution process of the proposed method. **a** MTD, **b** direct DPT, **c** MTD after SA, **d** extraction of the target signal after SA, and **e** DPT of the extracted signal

still serious, and it is difficult to accurately judge the target. Figure 6d is the target signal extracted by the proposed method, where the delay range is the area between the two red lines in Fig. 6c. Figure 6e shows the DPT result of the signal in Fig. 6d, and its output SNR is greatly improved compared with Fig. 6b, from which the target can be clearly found.

5.2 Simulation experiment

(1) Single target detection performance

We suppose the radar system parameters are the same as 4.1, the target speed is 1000 m/s, the acceleration is 15 m/s², its distance from the radar is 100 km, the SNR of the input signal is −25 dB, the speed compensation value is 500 m/s, and $\Delta\tau' = 20$. Figure 7a shows the MTD processing result of the echo signal, Fig. 7b depicts the processing result by the direct DPT, and Fig. 7c shows the processing result by the proposed

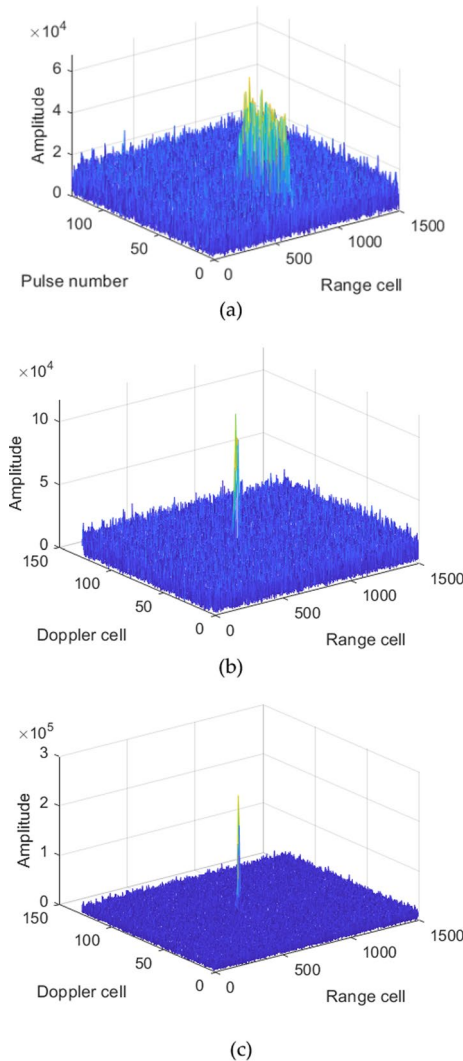


Fig. 7 Single target detection performance by different algorithms. **a** MTD, **b** direct DPT, and **c** proposed method

method. Compared with the results in Fig. 7, the MTD method still has obvious energy diffusion after speed compensation. The direct DPT method and the proposed method can achieve target detection, but the output SNR of the proposed method is larger, which is more conducive to improving the target detection probability and the parameter estimation accuracy.

(2) Multitarget detection performance

Two targets are assumed, with a speed of 1000 m/s, 1050 m/s, and an acceleration of 5 m/s^2 and 10 m/s^2 . The SNR of the input signals is -25 dB , and the speed compensation value is 500 m/s . $\Delta\tau' = 100$ and the other parameters are the same as in 4.1. Figure 8 shows that MTD causes serious energy diffusion. The direct DPT method can detect two targets, but it struggles with the Doppler spectrum spread. In contrast, the proposed method is capable of satisfactory detection of two targets, and the target resolution is the highest among the several methods.

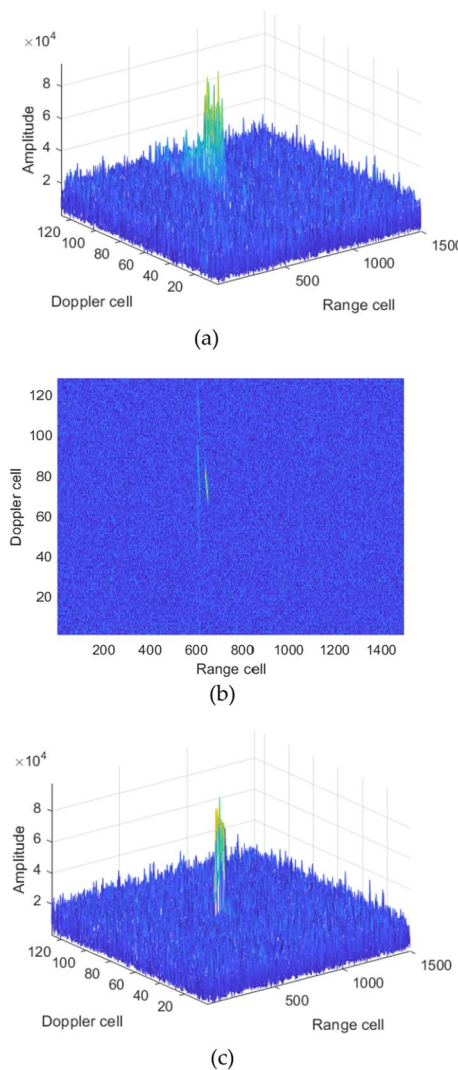


Fig. 8 Dual target detection performance of different methods. MTD, **b** Range-Doppler dimension in **a**, **c** the direct DPT, **d** Range-Doppler dimension in **c**, **e** the proposed method, **f** Range-Doppler dimension in **e**

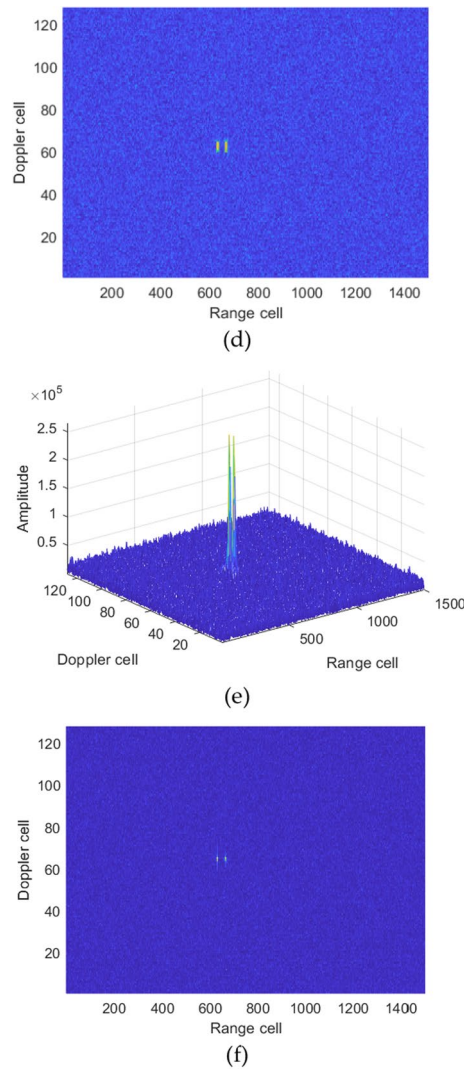


Fig. 8 continued

The above experiments show that the proposed method can effectively detect weak signals without accurate speed compensation and has a good compromise between detection performance and target resolution.

5.3 Verification with measured data

5.3.1 S-band radar data

To further verify the effectiveness of the method, the following measured data from aircrafts is used for analysis, and the white Gaussian noise that is added is -25 dB. The radar operates in the S band, the carrier frequency is 3 GHz, the signal bandwidth is 2 MHz, the pulse repetition time is 600 μ s, the pulse duration is 60 μ s, the integration pulse number is 2048, the sampling frequency is 4 MHz, the maximum speed of the target is 600 m/s, and the acceleration is 0.1 m/s². Figure 9 shows the processing results of the different methods, among which Fig. 9a shows the results of the MTD, from which it

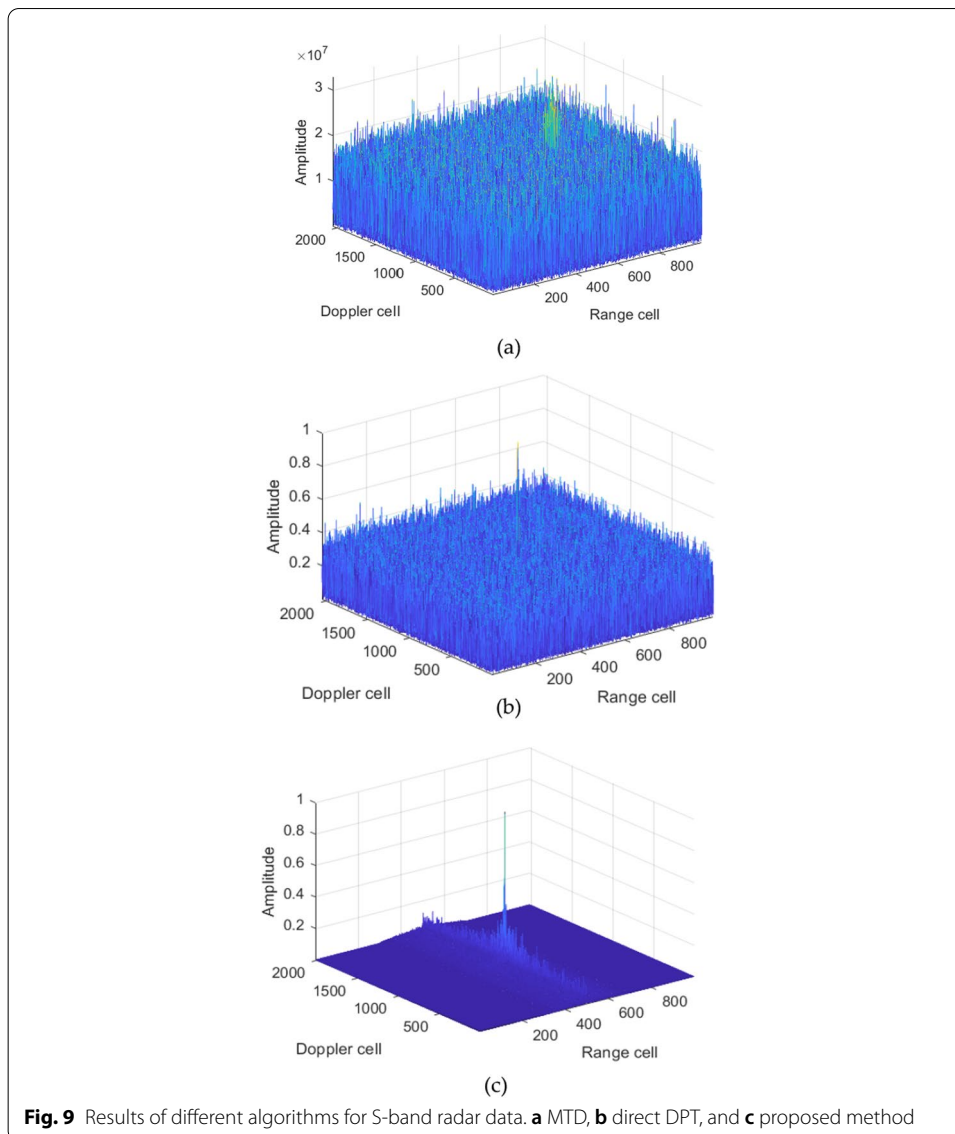


Fig. 9 Results of different algorithms for S-band radar data. **a** MTD, **b** direct DPT, and **c** proposed method

can be seen that the accumulated energy of the target signal is smaller, and the phenomenon of diffusion occurs. Figure 9b is the result of the direct DPT, from which the target can be observed, but the probability of a false alarm is relatively high. Figure 9c indicates the processing results of the proposed method, with the speed compensation value to be 300 m/s. After comparing the results of Fig. 9, it can be concluded that the proposed method can detect weak target signals, which verifies the effectiveness of the proposed method.

5.3.2 X-band radar data

The radar operates in the X-band, the transmission waveform is the LFM signal, the pulse repetition frequency is 10 kHz, the bandwidth is 2 GHz, and the accumulation time is 100 ms. Figure 10a shows the MTD results, Fig. 10b shows the MTD time-Doppler results, Fig. 11a shows the results of the proposed method with a compensation

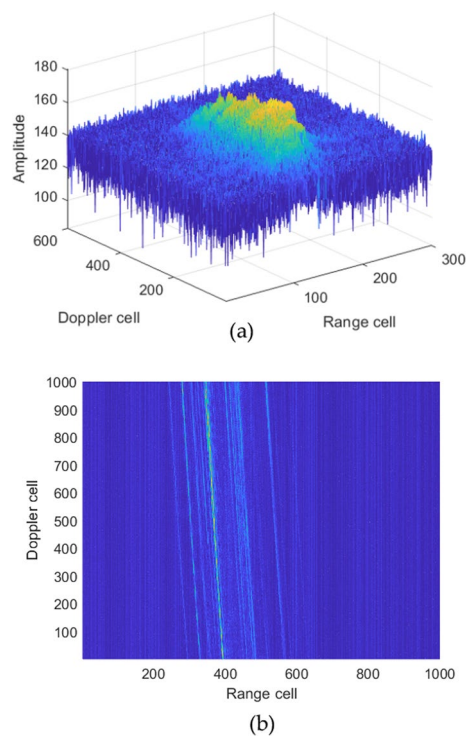


Fig. 10 Results of the MTD for X-band radar data. **a** MTD, **b** Range-Doppler

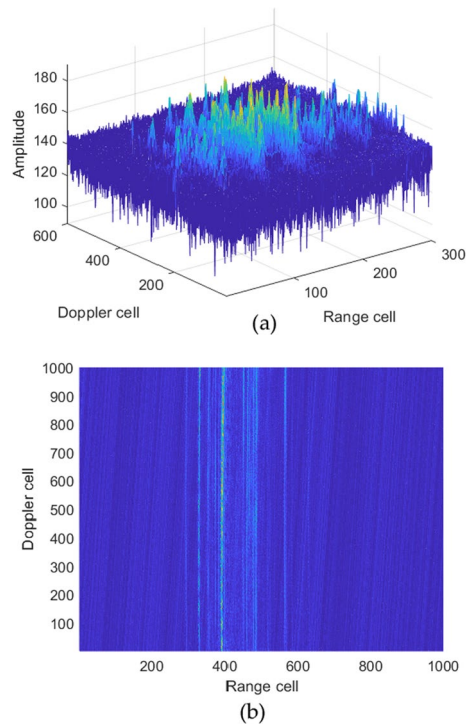


Fig. 11 Results of the proposed method for the X-band radar data. **a** The proposed method, **b** Range-Doppler

speed of 150 m/s, and Fig. 11b shows the time-Doppler results of the proposed method. Comparing Figs. 10 and 11, it can be seen that after the processing of the proposed method, the time-delay migration of the target is corrected, which is conducive to subsequent target detection and imaging processing.

6 Conclusion

Aiming at the problem of a large amount of computation in a highly manoeuvring target detection method, a hybrid coherent accumulation algorithm is proposed in this paper. This method combines the respective advantages of the parameter compensation method and the cross-correlation processing method. The specific performance data are summarized as follows: (1) The proposed method only needs to compensate for the target speed a few times, and then the DPT method can be used to obtain the target speed and the acceleration information. (2) The proposed method uses SA to obtain the time delay estimation range of the target, which can improve the output SNR of the DPT, which is not only conducive to improving the accuracy of parameter estimation but is also conducive to reducing the amount of operation. (3) The proposed method is applicable to the detection of uniformly accelerated targets. When the target is non-uniformly accelerated, the proposed method cannot be used directly. It needs to reduce the accumulation time or segment the non-uniform motion into uniform motion, which is also the focus of further research.

Abbreviations

SA: Scaling algorithm; MLE: Maximum likelihood estimator; RM: Range migration; KT: Keystone; RFT: Radon Fourier; TDST: Three-dimensional scaled transform; LVD: Lv's distribution; SFT: Sparse Fourier transform; DPT: Discrete polynomial-phase transform; ACCF: Adjacent cross correlation function; SNR: Signal-to-noise ratio.

Acknowledgements

The authors thank the anonymous reviewers for their enlightening comments and careful reviews, which helped improve the manuscript.

Author contributions

All authors contributed to the conception and design of the experiments and the interpretation of simulation results. PCS wrote the software, performed the experiments and data analysis, and wrote the first draft of the manuscript. HHL and GHL give some helpful experimental instructions and guidance. All authors read and approved the final manuscript.

Funding

This work was supported by Foundation Research Program of Shanxi Province of China under Grant No. 20210302123057.

Declarations

Competing interests

The authors declare that they have no competing interests.

Author details

¹National Key Laboratory of Electronic Measurement Technology, North University of China, Taiyuan 030051, China.

²Shanxi Key Laboratory of Information Detection and Processing, Taiyuan 030051, China.

Received: 29 December 2021 Accepted: 20 May 2022

Published online: 03 June 2022

References

1. X. Chen, J. Guan, X. Li, Y. He, Effective coherent integration method for marine target with micromotion via phase differentiation and radon-Lv's distribution. *IET Radar Sonar Navig.* **9**(9), 1284–1295 (2015)
2. P. Huang, G. Liao, Z. Yang, X. Xia, J. Ma, J. Ma, Long-time coherent integration for weak maneuvering target detection and high-order motion parameter estimation based on keystone transform. *IEEE Trans. Signal Process.* **64**(15), 4013–4026 (2015)

3. X. Chen et al., Sparse long-time coherent integration-based detection method for radar low-observable manoeuvring target. *IET Radar Sonar Navig.* **14**(4), 538–546 (2020)
4. Z. Sun et al., Coherent detection method for maneuvering target with complex motions. *J. Eng.* **2019**(21), 8032–8036 (2019)
5. J. Zheng, H. Liu, Q. Liu, Parameterized centroid frequency-chirp rate distribution for LFM signal analysis and mechanisms of constant delay introduction. *IEEE Trans. Signal Process.* **65**(24), 6435–6447 (2017)
6. X. Li, Z. Sun, W. Yi et al., Computationally efficient coherent detection and parameter estimation algorithm for maneuvering target. *Signal Process.* **155**, 130–142 (2019)
7. X. Li, Y. Zhong, B. Hu, Motion compensation for highly squinted SAR data based on azimuth nonlinear chirp scaling algorithm. In *2019 IEEE 5th International Conference on Computer and Communications (ICCC), Chengdu, China, 2019*, pp. 220–224
8. T.J. Abatzoglou, G.O. Gheen, Range, radial velocity, and acceleration MLE using radar LFM pulse train. *IEEE Trans. Aerosp. Electron. Syst.* **34**(4), 1070–1083 (1998)
9. R.P. Perry, R.C. DiPietro, R.L. Fante, Coherent integration with range migration using keystone formatting. In *Proceedings of IEEE Radar Conference, Boston, MA, USA*, pp. 863–868 (2007)
10. G. Sun, M. Xing, X. Xia, Y. Wu, Z. Bao, Robust ground moving target imaging using deramp-keystone processing. *IEEE Trans. Geosci. Remote Sens.* **51**(2), 966–982 (2013)
11. J. Zheng, T. Su, Q. Liu, ISAR imaging of targets with complex motion based on the keystone time-chirp rate distribution. *IEEE Geosci. Remote Sens. Lett.* **11**(7), 1275–1279 (2014)
12. J. Zheng, T. Su, H. Liu, G. Liao, Z. Liu, Q. Liu, Radar high-speed target detection based on the frequency-domain deramp-keystone transform. *IEEE J. Sel. Top. Appl. Earth Observ. Remote Sens.* **9**(1), 285–294 (2016)
13. R. Sharif, A. Saman, Efficient wideband signal parameter estimation using a Radon-ambiguity transform slice. *IEEE Trans. Aerosp. Electron. Syst.* **43**(2), 673–688 (2007)
14. J. Xu, J. Yu, Y. Peng, X. Xia, Radon-Fourier transform for radar detection, I: generalized Doppler filter bank. *IEEE Trans. Aerosp. Electron. Syst.* **47**(2), 1186–1200 (2011)
15. J. Yu, J. Xu, Y. Peng, X. Xia, Radon-Fourier transform for radar detection, III: optimality and fast implementations. *IEEE Trans. Aerosp. Electron. Syst.* **48**(2), 991–1004 (2012)
16. J. Xu et al., Radar maneuvering target motion estimation based on generalized Radon-Fourier transform. *IEEE Trans. Signal Process.* **60**(12), 6190–6201 (2012)
17. J. Zheng et al., Radar high-speed maneuvering target detection based on three-dimensional scaled transform. *IEEE J. Sel. Top. Appl. Earth Observ. Remote Sens.* **11**(8), 2821–2833 (2018)
18. X. Li, G. Cui, W. Yi, L. Kong, Fast coherent integration for maneuvering target with high-order range migration via TRT-SKT-LVD. *IEEE Trans. Aerosp. Electron. Syst.* **52**(6), 2803–2814 (2016)
19. R. Tao, N. Zhang, Y. Yang, Analysing and compensating the effects of range and Doppler frequency migrations in linear frequency modulation pulse compression radar. *IET Radar Sonar Navig.* **5**(1), 12–22 (2011)
20. X. Rao, H. Tao, J. Su, J. Xie, X. Zhang, Detection of constant radial acceleration weak target via IAR-FRFT. *IEEE Trans. Aerosp. Electron. Syst.* **51**(4), 214–224 (2016)
21. X. Chen, J. Guan, N. Liu, Y. He, Maneuvering target detection via Radon-fractional Fourier transform-based long-time coherent integration. *IEEE Trans. Signal Process.* **62**(4), 939–953 (2014)
22. C. Pang, T. Shan, R. Tao, N. Zhang, Detection of high-speed and accelerated target based on the linear frequency modulation radar. *IET Radar Sonar Navig.* **8**(1), 37–47 (2014)
23. S. Liu, T. Shan, R. Tao et al., Sparse discrete fractional Fourier transform ants applications. *IEEE Trans. Signal Process.* **62**(24), 6582–6595 (2014)
24. C. Pang, S. Liu, Y. Han, High-speed target detection algorithm based on sparse Fourier transform. *IEEE Access* **6**, 37828–37836 (2018)
25. W. Wu, G. Wang, J. Sun, Polynomial Radon-polynomial Fourier transform for near space hypersonic maneuvering target detection. *IEEE Trans. Aerosp. Electron. Syst.* **54**(3), 1306–1322 (2018)
26. S. Peleg, B. Friedlander, The discrete polynomial-phase transform. *IEEE Trans. Signal Process.* **43**(8), 1901–1914 (1995)
27. S. Liu, T. Shan, Y.D. Zhang, R. Tao, Y. Feng, A fast algorithm for multicomponent LFM signal analysis exploiting segmented DPT and SDFrFT. In *Proceedings of IEEE International Radar Conference, Arlington, VA, USA, May 2015*, pp. 1139–1143
28. C.S. Pang, S.H. Liu, Y. Han, Coherent detection algorithm for radar maneuvering targets based on discrete polynomial-phase transform. *IEEE J. Sel. Top. Appl. Earth Observ. Remote Sens.* **12**(9), 3412–3422 (2019)
29. Z. Niu, J. Zheng, T. Su, J. Zhang, Fast implementation of scaled inverse Fourier transform for high-speed radar target detection. *Electron. Lett.* **53**(16), 1142–1144 (2017)
30. J. Zheng, T. Su, W. Zhu et al., Radar high-speed target detection based on the scaled inverse Fourier transform. *IEEE J. Sel. Top. Appl. Earth Observ. Remote Sens.* **8**(3), 1108–1109 (2015)
31. X.L. Li, G.L. Cui, W. Yi, L.J. Kong, A fast maneuvering target motion parameters estimation algorithm based on ACCF. *IEEE Signal Process. Lett.* **22**(3), 270–274 (2015)
32. X. Li, G. Cui, L. Kong et al., Fast non-searching method for maneuvering target detection and motion parameters estimation. *IEEE Trans. Signal Process.* **64**(9), 2232–2244 (2016)
33. J. Zhang, T. Su, J. Zheng, X. He, Novel fast coherent detection algorithm for radar maneuvering target with jerk motion. *IEEE J. Sel. Top. Appl. Earth Observ. Remote Sens.* **10**(5), 1108–1119 (2017)

Publisher's Note

Springer Nature remains neutral with regard to jurisdictional claims in published maps and institutional affiliations.